The Journal of Chemical Physics

RESEARCH ARTICLE | AUGUST 29 2024

Dynamics of the Cl + CH_3CN reaction on an automatically-developed full-dimensional *ab initio* potential energy surface

Petra Tóth ; Tímea Szűcs ; Tibor Győri ; Gábor Czakó

J. Chem. Phys. 161, 084304 (2024)
https://doi.org/10.1063/5.0220917

The Journal of Chemical Physics ARTICLE pubs.aip.org/aip/jcp

Dynamics of the Cl + CH_3CN reaction on an automatically-developed full-dimensional *ab initio* potential energy surface

Cite as: J. Chem. Phys. 161, 084304 (2024); doi: 10.1063/5.0220917
Submitted: 29 May 2024 • Accepted: 11 August 2024 •
Published Online: 29 August 2024

Petra Tóth, Tímea Szűcs, Tibor Győri, and Gábor Czakó[a]

AFFILIATIONS

MTA-SZTE Lendület Computational Reaction Dynamics Research Group, Interdisciplinary Excellence Centre and Department of Physical Chemistry and Materials Science, Institute of Chemistry, University of Szeged, Rerrich Béla tér 1, Szeged H-6720, Hungary

[a]Author to whom correspondence should be addressed: gczako@chem.u-szeged.hu

ABSTRACT

A full-dimensional analytical potential energy surface (PES) is developed for the Cl + CH_3CN reaction following our previous work on the benchmark *ab initio* characterization of the stationary points. The spin–orbit-corrected PES is constructed using the ROBOSURFER program and a fifth-order permutationally invariant polynomial method for fitting the high-accuracy energy points determined by a ManyHF-based coupled-cluster/triple-zeta-quality composite method. Quasi-classical trajectory simulations are performed at six collision energies between 10 and 60 kcal mol^{-1}. Multiple low-probability product channels are found, including isomerization to isonitrile (CH_3NC), but out of the eight possible channels, only the H-abstraction has significant reaction probability; thus, detailed dynamics studies are carried out only for this reaction. The cross sections and opacity functions show that the probability of the H-abstraction reaction increases with increasing collision energy (E_{coll}). Scattering angle, initial attack angle, and product relative translational energy distributions indicate that the mechanism changes with the collision energy from indirect/rebound to direct stripping. The distribution of initial attack angles shows a clear preference for methyl group attack but with different angles at different E_{coll} values. Post-reaction energy distributions show that the energy transfer is biased toward the products' relative translational energy instead of their internal energy. Rotational and vibrational energy have about the same amount of contribution to the internal energy in the case of both products (HCl and CH_2CN), i.e., both of them are formed with high rotational excitations. HCl is produced mostly in the ground vibrational state, while a notable fraction of CH_2CN is formed with vibrational excitation.

I. INTRODUCTION

Moving beyond traditional kinetics studies, modern experimental and theoretical techniques can investigate chemical reactions under single-collision conditions, thereby providing insights into the atomic-level dynamics and mechanisms of processes. Such techniques are the crossed-beam experiments and the quasi-classical trajectory (QCT) or quantum scattering computations, which have been frequently used to investigate the dynamics of fundamental chemical reactions to uncover the basic rules of reactivity. Among the benchmark systems, the reactions of the chlorine atom (Cl) with small molecules have played a central role in recent decades.[1–20] For example, many groups, in most cases including ours, studied the reaction dynamics of Cl with CH_4,[3–10] C_2H_6,[11–14] CH_3OH,[15–17] and CH_3NH_2.[18,19] In the present study, we plan to extend the previous work by investigating the Cl + CH_3CN reaction using first-principles theory. This reaction has only been investigated by traditional kinetics methods, providing rate constants with experimental and transition-state-theory-based approaches[21–27] as well as with anion photo-detachment spectroscopy[28] and computations.[29] The scattering dynamics of the title reaction has never been studied unlike in the case of the above-mentioned other reactions of the Cl atom. Furthermore, for the similar F + CH_3CN system, both experimental and theoretical dynamics investigations were reported.[30–33] Therefore, in order to extend our knowledge on the dynamics of fundamental polyatomic reactions, we started to investigate the Cl + CH_3CN system in 2022.[34] Using high-level *ab initio* methods, we characterized the stationary points of the potential

energy surface (PES) of the title reaction, revealing several reaction pathways and product channels and computing their benchmark relative energies.[34] Here, we plan to move beyond the static picture and provide a detailed dynamics investigation for the Cl + CH_3CN reaction, thereby uncovering the competition between the different channels and motivating and guiding future experiments.

For a seven-atomic system, such as the title reaction, one usually uses the QCT method to describe the dynamics in full dimensions. Within the QCT approach, two main ways exist to proceed: (1) one may carry out direct dynamics simulations, where the gradients are computed on-the-fly using an electronic structure program package, or (2) a PES is developed by fitting *ab initio* data, which allows efficient trajectory computations. The direct dynamics approach was used for the F + CH_3CN system by Hase and co-workers.[33] In our group, we follow the fitted-PES-based approach as this latter technique allows using higher levels of *ab initio* theory and running orders of magnitude more trajectories, providing more accurate results from both electronic-structure and statistical aspects. Of course, the development of a full-dimensional global PES can provide several challenges, for example, sampling the appropriate nuclear configurations and finding a robust electronic structure method are usually not straightforward. In order to overcome these difficulties, the ROBOSURFER program package[35] and the ManyHF method[36] were developed in our group, which will be used in the present study as well. The details of the computations are described in Sec. II, the results are given and discussed in Sec. III, and this paper ends with a summary and conclusions in Sec. IV.

II. COMPUTATIONAL DETAILS

The full-dimensional analytical potential energy surface (PES) development begins with the characterization of the stationary points of the PES. The seven pathways of the Cl($^2P_{3/2}$) + CH_3CN reaction were examined in our previous work,[34] reporting the stationary-point geometries as well as the benchmark classical and adiabatic energies of the products, post-reaction complexes (MINs), and transition states (TSs) relative to the reactants. These energies were determined using an unrestricted explicitly-correlated coupled-cluster singles, doubles, and perturbative triples method (UCCSD(T)-F12b)[37] with the aug-cc-pVQZ basis set[38] at the UCCSD(T)-F12b/aug-cc-pVTZ geometries. All UCCSD(T)-F12b computations used restricted open-shell Hartree–Fock (ROHF) reference wavefunctions. Further energy contributions were also taken into account. The hydrogen abstraction (H Abs, leading to HCl + CH_2CN) is the only exothermic reaction path; however, it also has a small barrier with a classical(adiabatic) relative energy of 8.15(3.76) kcal mol^{-1}. All other pathways are endothermic. Both the hydrogen-substitution (H sub, leading to H + $ClCH_2CN$) and cyano-substitution (CN sub, leading to CN + CH_3Cl) reactions can proceed via a Walden inversion (W) or a front-side attack (FS) transition state. In the case of methyl-substitution (CH_3 sub, leading to CH_3 + CNCl/ClCN), two different outcomes are possible, depending on which atom of the CN group is bonded to Cl.

Based on the stationary-point structures mentioned above, initial fitting-set geometries are generated using a random displacement method. For each of the post-reaction complexes and transition states, 200 geometries are created by randomly displacing the Cartesian coordinates within a range of 0–0.32 Å. For the reactants and products, the same procedure is applied, but these two-fragment systems are also scattered randomly around each other, ensuring that their center of mass distances are between 3 and 8 Å, and we generate 500 geometries for each channel. At the resulting structures, single-point energy calculations are performed using the ROHF-UCCSD(T)-F12a/cc-pVDZ-F12 level of theory.[37,39] To minimize basis set errors, an additive correction based on the restricted explicitly-correlated second-order Møller–Plesset perturbation theory (RMP2-F12)[40] is used with the cc-pVTZ-F12 and the cc-pVDZ-F12 basis sets.[39] In the reactant region, many calculations failed due to ROHF convergence problems; therefore, the ManyHF method[36] was used in the computations to reliably obtain the lowest-energy ROHF wavefunction. Based on the above-described *ab initio* computations, a high-level composite energy is determined for each geometry, defined as

$$\begin{aligned} E_{\text{composite}} = {} & \text{ManyHF-UCCSD(T)-F12a/cc-pVDZ-F12} \\ & + \text{ManyHF-RMP2-F12/cc-pVTZ-F12} \\ & - \text{ManyHF-RMP2-F12/cc-pVDZ-F12}. \end{aligned} \tag{1}$$

The results obtained using the ManyHF-based composite method are in good agreement with the default HF-based results, with an average deviation of around 0.1 kcal mol^{-1}. The largest difference observed is just 2.1 kcal mol^{-1}. In contrast, in other studies, such as the reaction of Cl + CH_3NH_2, the error was far more significant, with the most frequent default HF error value being around 90 kcal mol^{-1}.[19] Although the difference in energy values for our system would not justify using the ManyHF method, the success rate of the calculations shows that only about half of the default-algorithm-based ROHF computations in the reactant region were successful compared to 91% for ManyHF-based ones.

The single-point energy calculations result in an initial database containing 5424 energy points. After discarding chemically irrelevant geometries with relative energies higher than 200 kcal mol^{-1} compared to the global minimum, the database contains 4261 *ab initio* points. The permutationally invariant polynomial (PIP) method[41] is used for fitting, ensuring that the PES is invariant under the permutation of like atoms. A full-dimensional analytical Morse-like function is used to represent the PES, which is constructed by expanding polynomials of $y_{ij} = \exp(-r_{ij}/a)$, where r_{ij} are the atom–atom distances. The diffuseness of the polynomial fitting basis is controlled by the a parameter, which is set to 2.5 bohrs for this system. During the initial stages of development, a fourth-order polynomial is used because the initial PES database contains fewer energy points than the number of coefficients required for a fifth-order fit. To compute a fourth-order expansion, 1798 coefficients are used, whereas a fifth-order expansion results in 7970 coefficients. A weighted least-squares fit is performed using a weight of

$$w(E) = \frac{E_0}{E + E_0} \cdot \frac{E_1}{E + E_1} \tag{2}$$

for the potential energy of the geometry (E) relative to the global minimum, where E_0 and E_1 are set to 0.1 and 0.5 hartree, respectively. The use of $w(E)$ gives larger weights for the chemically relevant low-energy part of the data points and suppresses the effects of the less-important high-energy points. E_0 is chosen to be around 60 kcal mol^{-1}, providing a weight of around 0.5 for the highest-lying

stationary-point regions, whereas E_1 is usually set to a very high value (314 kcal mol^{-1} in the present case) to suppress the extremely high-energy points more drastically. Note that the initial dataset does not contain points with energies greater than 200 kcal mol^{-1} relative to the global minimum; however, during the further PES development (see below), some higher-energy points may be added to the fitting set, which have small weights but may become useful to prevent any unphysical behavior of the PES, for example, breakdowns at short interatomic distances.

The quality of the PES is improved through an iterative process that is facilitated by the ROBOSURFER program package[35] developed in our group. New geometries are generated using quasi-classical trajectory (QCT) simulations. Quantum chemical inputs are automatically set up for selected structures at the user-requested level of theory. If any new geometries exceed the threshold fitting error, they are added iteratively to the fitting set after further filtering. During the present PES development, the collision energy (E_{coll}) used in the QCT computations is varied from 10 to 100 kcal mol^{-1}, with an increment of 10 kcal mol^{-1}. For each E_{coll} value, trajectories are run with different impact parameters (b) ranging from 0 to 8 bohrs, with a step size of 0.5 bohr. The targeted fitting error in ROBOSURFER is 0.5 kcal mol^{-1}. Over the course of development, the fraction of unphysical trajectories was one of the primary methods for evaluating the quality of the PES. Unphysical trajectories are defined as trajectories that form energetically unfeasible products, often through a violation of energy conservation that happens if a trajectory enters a region of the PES where unphysically large gradients are present. As PES development progresses, such regions are gradually corrected by ROBOSURFER, resulting in much fewer unphysical trajectories, which signals that any remaining severely unphysical regions are no longer dynamically accessible. Whenever this happens, E_{coll} is raised to make the sampling of higher energy regions of the PES possible, and further ROBOSURFER iterations are run until the fraction of unphysical trajectories reduces again. After 535 iterations, the PES contains 8288 energy points; therefore, fifth-order fitting can be used to continue development with the same E_{coll} and b values as at the beginning. The final non-relativistic PES is accepted after 658 iterations, made up of 11 221 geometries and the corresponding energies. Due to the open-shell nature of the system, the PES needs to be enhanced by the relativistic spin–orbit (SO) correction to achieve chemical accuracy because of the energy-lowering effect of the chlorine atom's SO splitting. The Davidson-corrected[42] all-electron multi-reference configuration interaction method[43] (MRCI+Q) is used combined with the aug-cc-pwCVDZ basis set[44] and applying the interacting states approach[45] considering three doublet electronic states. For the three-state state-averaged MCSCF reference computations, we use an active space of five electrons on three spatial orbitals, which corresponds to the three 3p-like orbitals of the Cl atom in the reactant region. For each geometry, the final potential energy is computed as

$$E_{\text{composite}} + \Delta_{\text{SO}}(\text{MRCI+Q}(5,3)/\text{aug-cc-pwCVDZ}), \quad (3)$$

where the SO effect (Δ_{SO}) is calculated as the difference between the SO_1 and the non-SO_1 ground-state potential energies. In nine cases, MCSCF convergence problems occurred; therefore, the final PES coefficients are obtained by fitting a fifth-order polynomial to 11 212 *ab initio* energy points. All the electronic structure computations needed for the PES development are carried out with the MOLPRO 2015.1 program package.[46]

Quasi-classical dynamics simulations are performed using our own Fortran program interfaced with the final PES at collision energies of 10, 20, 30, 40, 50, and 60 kcal mol^{-1} with b impact parameter values from 0 to 8 bohrs with steps of 0.5 bohr. The molecular reactant is given zero-point energy (ZPE) by choosing the initial positions and velocities of its atoms to correspond to the ground vibrational state using normal-mode sampling.[47] The distance between the Cl atom and the CH_3CN molecule is set using the formula $\sqrt{x^2 + b^2}$, where x = 18.90 bohrs (10 Å), and the orientations of the reactants are randomly rotated. Each trajectory is propagated using the velocity Verlet method (with numerical forces) and a time step of 0.0726 fs until the largest interatomic distance exceeds the largest initial one by 1 bohr. At each collision energy and impact parameter, 5000 trajectories were propagated, resulting in a total of 510 000 simulations.

III. RESULTS AND DISCUSSION

The quality of the potential energy surface can be assessed with the root-mean-square (rms) error of the fitting. In our case, the rms values are 0.73, 1.12, and 0.88 kcal mol^{-1} within the 0.00–62.75, 62.75–125.50, and 125.50–313.75 kcal mol^{-1} intervals, relative to the global minimum of the dataset, respectively. This means that in the most relevant lowest-energy region, the rms value falls within 1 kcal mol^{-1}, the traditional threshold for chemical accuracy. The distribution of the fitting errors shown in Fig. S1 of the supplementary material also indicates good accuracy as basically all the *ab initio* points in the lowest interval (0.00–62.75 kcal mol^{-1}) are reproduced by the PES values within 2 kcal mol^{-1}. The largest absolute fitting error of all data is ~13 kcal mol^{-1}; however, that point is above the global minimum by more than 100 kcal mol^{-1}. Figure 1 shows the stationary points of the potential energy surface for the seven reaction channels with the benchmark[34] and composite classical relative energies compared to the PES-optimized energies of the stationary points, relative to the reactants. The benchmark values are taken from Ref. 34, where they were determined as

$$\begin{aligned}\Delta E_{\text{benchmark}} = {} & \text{ROHF-UCCSD(T)-F12b/aug-cc-pVQZ} \\ & + \delta[\text{UHF-UCCSDT}] + \delta[\text{UHF-UCCSDT(Q)}] \\ & + \Delta_{\text{core}} + \Delta_{\text{rel}} + \Delta_{\text{SO}}, \end{aligned} \quad (4)$$

where δ[UHF-UCCSDT] + δ[UHF-UCCSDT(Q)], Δ_{core}, Δ_{rel}, and Δ_{SO} denote post-CCSD(T), core correlation, scalar relativistic, and SO corrections, respectively.[34] For the most important H-abstraction reaction, the relative energy values are in good agreement: for the products, the $[\Delta E_{PES} - \Delta E_{benchmark}(E_{composite} + \Delta_{SO})]$ error is only 0.59(0.62) kcal mol^{-1}, while for the transition state and the post-reaction complex, the absolute differences are also small, 0.57(0.11) and 0.48(0.14) kcal mol^{-1}, respectively. This is the only exothermic pathway of the system; therefore, it is important for the dynamics that the PES represents this region accurately. In the case of the higher-energy stationary points, the error is mostly under or around 1 kcal mol^{-1}; thus, these are also within chemical accuracy. The average absolute difference between the $\Delta E_{benchmark}(E_{composite} + \Delta_{SO})$ and ΔE_{PES} energies for all stationary points is 0.93(0.78)

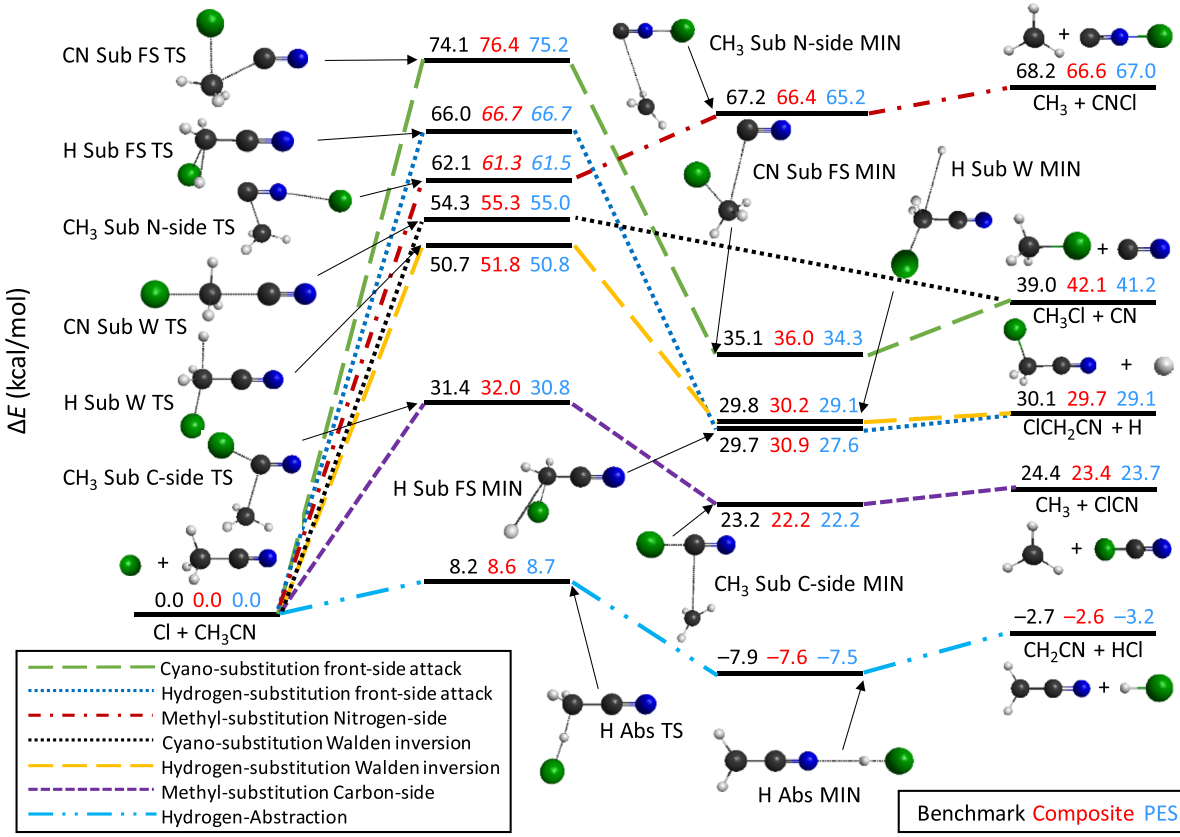

FIG. 1. Schematic potential energy diagram of the Cl($^2P_{3/2}$) + CH_3CN reaction with the benchmark classical energies [Eq. (4)],[34] composite values [Eq. (3)] obtained at geometries optimized on the PES, and the corresponding PES values. Italic energies correspond to ROHF-UCCSD(T)-F12b/aug-cc-pVTZ geometries. All energies are given in kcal mol^{-1}, relative to the reactants.

kcal mol^{-1}. It is also important to note that the $\Delta E_{PES} - \Delta E_{benchmark}$ errors arise from a combination of both the fitting error [$\Delta E_{PES} - \Delta(E_{composite} + \Delta_{SO})$] and the limitations of the level of theory used for the *ab initio* computations. We can state that the newly-developed analytical potential energy surface describes the title multi-channel system well.

To further support the above conclusion on the accuracy of the PES, we compare the most relevant structural parameters obtained on the PES with ROHF-UCCSD(T)-F12b/aug-cc-pVTZ reference values,[34] as shown in Fig. S2 of the supplementary material. We can say that the PES reproduces well the *ab initio* data considering the floppiness of certain stretching and bending coordinates. For example, the tight bond lengths (C–H and C–C of the reactant, etc.) are usually described within 0.001–0.01 Å, whereas the flexible coordinates (C···H in H Sub W MIN, C···C in CN Sub FS MIN, etc.) may have larger deviations of around 0.1 Å.

The potential energy curves along various Cl···CH_3CN axes can be seen in Fig. 2. The PES relative energies are in good agreement with the direct composite *ab initio* ones as in most cases, the differences are within the rms error. In addition, the depths of the minima are usually well reproduced by the PES, and their locations are sometimes just a bit shifted, but this is understandable in light of the flatness of the PES. It also can be seen that the potentials converge well to the asymptotic limits and the curves are usually smooth; thus, long-range interactions are accurately described. The small bump along the Cl···H_3CCN C_3 axis has a magnitude comparable to the rms fitting error and does not go significantly above the asymptotic limit; thus, we do not expect any observable dynamical effect of this artifact.

The trajectories from the QCT simulations are analyzed starting with the classification of different reaction channels using the coordinates of the products in order to determine the reaction probabilities. The opacity function [$P(b)$] is the reaction probability as a function of the b impact parameter, and the integral cross section (ICS, σ) is the b-weighted numerical integral of $P(b)$. Except for the hydrogen-abstraction pathway, the reaction probabilities are negligible, in most cases, the ICS values are <0.01 $bohr^2$. In the case of the carbon-side methyl-substitution, at higher collision energies, there is a small probability of the reaction (σ = 0.0669 $bohr^2$, E_{coll} = 60 kcal mol^{-1}), but this reactivity is much smaller than for the hydrogen-abstraction at the same E_{coll} (σ = 16.59 $bohrs^2$). Therefore, in this study, more detailed dynamics results are reported only for

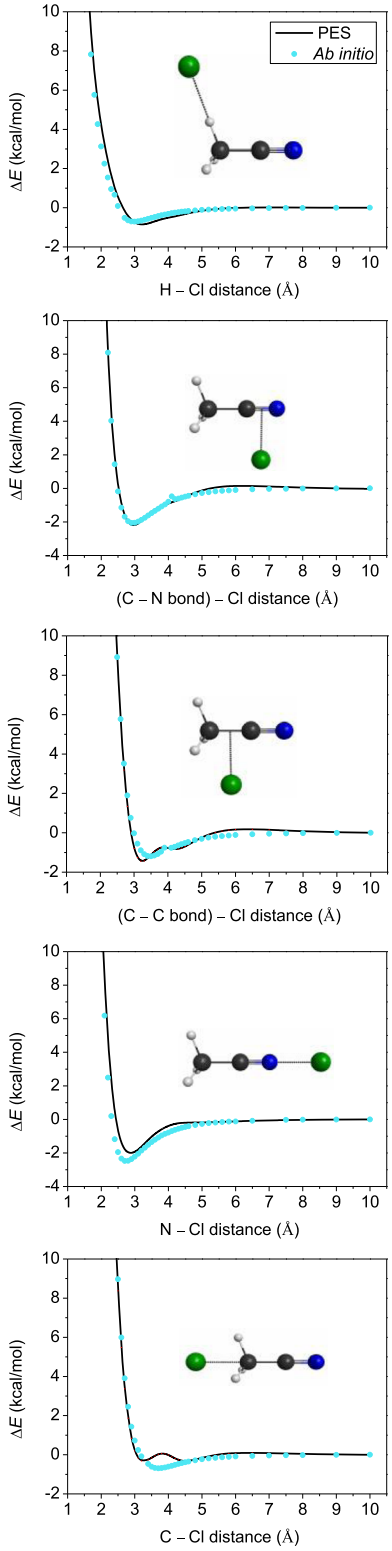

FIG. 2. Potential energies along various axes for the Cl + CH_3CN reaction, obtained on the present PES and by the composite *ab initio* level of theory [Eq. (3)].

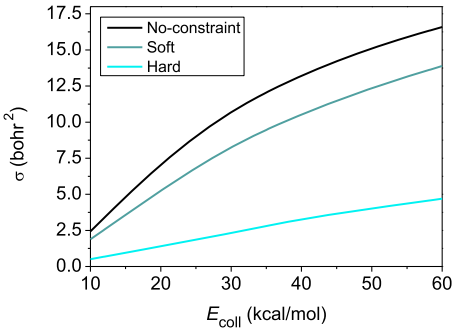

FIG. 3. Integral cross sections as a function of the collision energy for the Cl + CH_3CN hydrogen-abstraction reaction with and without soft or hard ZPE constraint.

the major H-abstraction reaction. It is interesting to note that during the analysis of the initially unclassifiable trajectories, a new reaction pathway appeared, where the approach of the Cl atom causes the isomerization of the CH_3CN molecule resulting in a CH_3NC product. In the first step of this mechanism, the chlorine atom attaches to the carbon atom of the CN group, loosening the carbon–carbon bond, but fails to fully detach the cyano group. Instead, the group turns, and the nitrogen atom bonds to the carbon atom, while the chlorine atom moves apart from the now isomerized reactant molecule. However, the reaction probability for this isonitrile formation pathway is extremely low as it happens only in 15 cases out of all trajectories.

The integral cross sections as a function of collision energy for the H-abstraction reaction can be seen in Fig. 3. The increasing trend of the excitation function is consistent with the positive barrier of the abstraction process. Soft and hard zero-point energy restrictions are also applied, where in the soft case, the sum of the zero-point energies of the products has to be lower than the sum of their vibrational energies, while in the case of the hard constraint, each product has to fulfill this condition separately,

$$\text{soft:}\quad \mathrm{ZPE(HCl)} + \mathrm{ZPE(CH_2CN)} < E_{\mathrm{vib}}(\mathrm{HCl}) + E_{\mathrm{vib}}(\mathrm{CH_2CN}), \tag{5}$$

$$\text{hard:}\quad \mathrm{ZPE(HCl)} < E_{\mathrm{vib}}(\mathrm{HCl}) \text{ and } \mathrm{ZPE(CH_2CN)} < E_{\mathrm{vib}}(\mathrm{CH_2CN}). \tag{6}$$

If trajectories that violate the constraint are excluded from analysis, then with the soft constraint, the ICS values decrease by around 20%, whereas in the hard case, the change is far more significant, at around 75%. To estimate the statistical uncertainty of the ICS values, we analyze half of the trajectories. Table S1 in the supplementary material shows that the full and the half analyses provide basically the same cross-section values, and the relative H-abstraction ICS differences are always less than 2%, except for the lowest two collision energies with hard constraint, where the absolute cross sections are the smallest.

Figure 4 shows the opacity functions of the H-abstraction reaction at different collision energies, and the corresponding numerical data are given in Table S2 of the supplementary material. It can

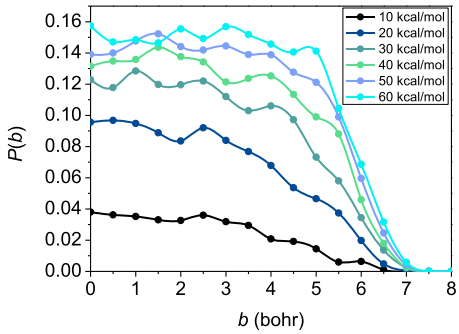

FIG. 4. Reaction probabilities as a function of the impact parameter for the Cl + CH_3CN hydrogen-abstraction reaction obtained at different collision energies.

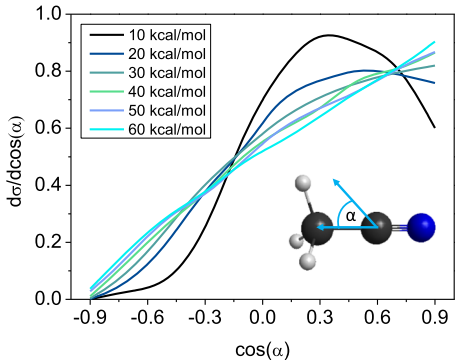

FIG. 6. Normalized initial attack angle distributions at different collision energies for the Cl + CH_3CN hydrogen-abstraction reaction.

be seen, as in the ICS graph, that with higher collision energy the reaction probability increases, for example, at E_{coll} = 10 kcal mol^{-1}, the $P(b)$ value is around 4%, while at 60 kcal mol^{-1} collision energy, the probability is around 16%. The b impact parameter also affects the $P(b)$ values, but this effect decreases as one moves toward higher collision energies. As shown in Fig. 4, at lower collision energies, the opacity function has an almost monotonous decay, but with higher E_{coll}, the $P(b)$ values plateau near a given value with the increasing impact parameter, until getting close to b_{max} (the highest b value where non-zero reaction probability occurs), where the decrease happens suddenly. This trend suggests that the direct stripping mechanism gets more and more dominant with increasing collision energy as the higher b values are getting more preferred.

The scattering angle (Θ) represents the angle between the velocity vectors of the center of masses of the products and reactants, as illustrated in Fig. 5. At low collision energies, the scattering is quite isotropic, suggesting the indirect character of the reaction. In contrast, with increasing collision energy, forward scattering becomes more and more dominant, which indicates that the reaction mechanism shifts toward direct stripping. At lower E_{coll}, we note a remarkably lowered cross section for near-perfectly forward-scattered [cos(Θ) ≈ 1] trajectories. This can be explained by the centrifugal potential, which hinders reactivity at lower E_{coll} and higher b values; thus, in these cases, forward scattering is less likely to happen.

The distributions of the initial attack angle for the hydrogen abstraction are shown in Fig. 6. The α angle is defined as 0° when the Cl atom attacks from the direction of the methyl group and 180° when it approaches from the nitrogen atom in line with the C–C bond. Based on the shape of the curves, it appears that there is a distinct preference for attack on the methyl group side, but also at lower collision energies, there is a peak around 0.3 cos(α) value. This angle (α ≈ 70°) corresponds to a near 180° Cl–H–C-angle attack on one of the hydrogen atoms, which is also reflected in the geometry of the transition state. This angle preference decreases with increasing collision energy and can be explained by the mechanism of the reaction at higher E_{coll}. As demonstrated by the scattering angle distribution as well, at lower collision energies, the reaction is indirect, and the rebound mechanism is more prominent. However, at higher E_{coll} values, the reaction becomes more direct, and the stripping mechanism becomes dominant, favoring α ≈ 0°.

We investigate the relative translational energy distributions of the products (HCl + CH_2CN) at six collision energies, as shown in Fig. 7. Considering the shape of the curves, it can be noted that with increasing E_{coll}, the peak of the curves drifts from the lowest

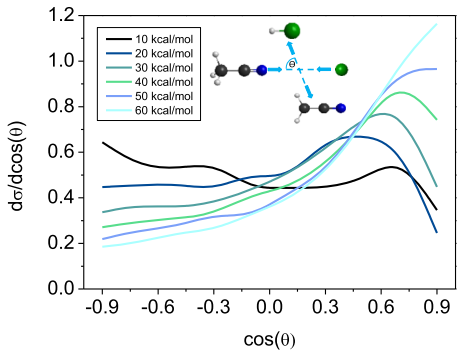

FIG. 5. Normalized scattering angle distributions at different collision energies for the Cl + CH_3CN hydrogen-abstraction reaction.

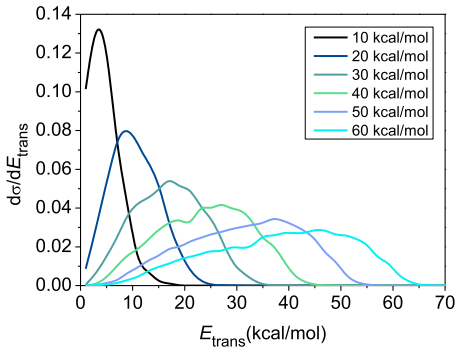

FIG. 7. Normalized relative translational energy distributions of the products at different collision energies for the hydrogen-abstraction channel of the Cl + CH_3CN reaction.

toward the highest available E_{trans} values. This phenomenon supports our claim that the reaction becomes more and more direct with increasing E_{coll} in accord with the scattering and attacking angle distributions. In addition, the shift of the maxima of the curves corresponds to the increment of the collision energy (the distance of the peaks is around 10 kcal mol^{-1}), showing efficient translational energy transfer between the reactants and products.

Figure 8 shows the internal energy (E_{int}) distributions for the hydrogen-abstraction products (HCl and CH_2CN), as well as the vibrational (E_{vib}) and rotational (E_{rot}) contributions to E_{int}. Considering the internal energy diagram of the HCl molecule, it can be seen that the distributions have a very small collision energy dependence; thus, the internal energy transfer from E_{coll} to this product is negligible compared to the contribution to E_{trans}. In the case of the CH_2CN product, at low collision energies, the peak is near the largest available energy, while at higher E_{coll}, the maximum is shifted to the smaller available energies. This effect also supports the indirect–direct transition in the mechanism with the increasing collision energies. A larger fraction of E_{coll} is transferred to the internal energy of CH_2CN, but this is still much smaller than the contribution to E_{trans}. Both HCl and CH_2CN are predominantly formed with internal energies greater than their respective ZPEs. Hydrogen abstraction is an energy-releasing reaction, but the contribution of the reaction heat to internal or translational energy is uncertain as it is only slightly exothermic (see Fig. 1). The smaller or larger collision energy dependence of the internal energies of the products is coming from the rotational energy as it can be seen in Fig. 8. The rotational quantum number (J) distribution for HCl also shows the non-significant E_{coll} dependence. In the case of CH_2CN, the $P(J)$ curves have large oscillations, but these are only due to statistical reasons because of the large number of J values. The collision energy dependence is well represented in the J values too. The vibrational energy distributions also indicate that the dependence on collision energy of the product's internal energies does not originate from E_{vib}

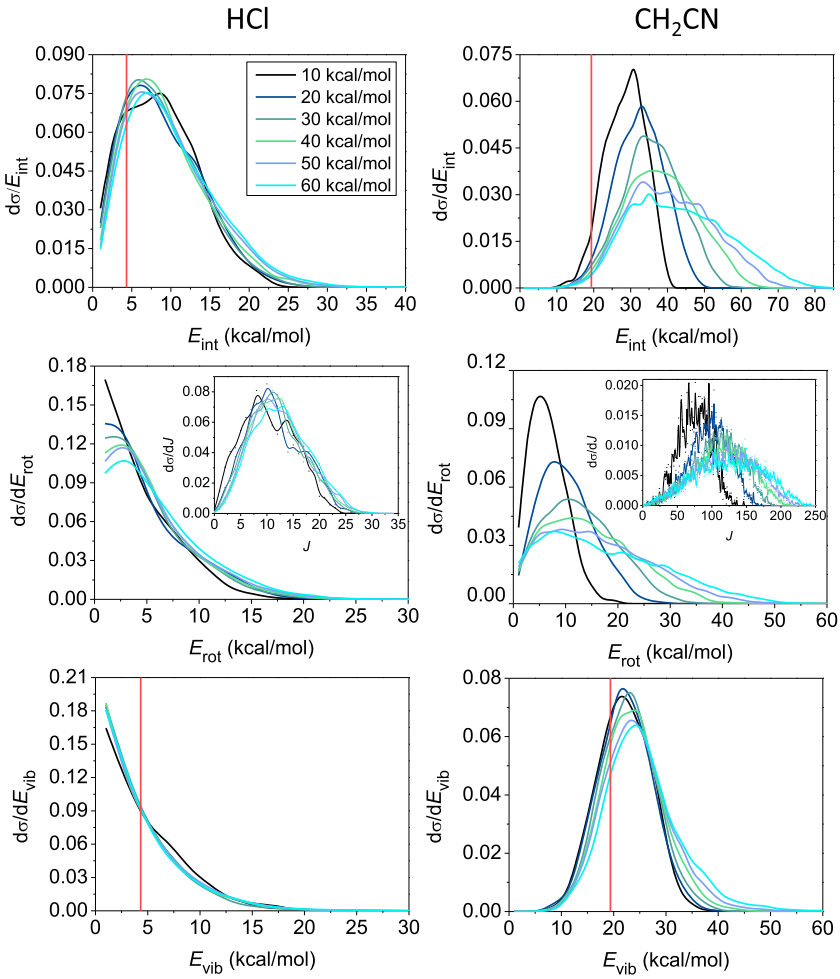

FIG. 8. Normalized internal (E_{int}), rotational (E_{rot}), vibrational (E_{vib}) energy, and rotational quantum number (J) distributions for the products of the Cl + CH_3CN H-abstraction reaction obtained at different collision energies. The ZPE values are shown as vertical lines.

because these E_{vib} curves remain mostly unchanged with variations in E_{coll}. Separating E_{int} to its E_{vib} and E_{rot} components also reveals that almost half of the HCl products have a lower vibrational energy than the ZPE, indicating a substantial prevalence of ZPE violation, which is also significant for the CH_2CN product. The majority of the trajectories result in a vibrationally ground state HCl molecule since the ZPE (4.32 kcal mol^{-1}) suggests that the first excited state has a vibrational energy of about 13 kcal mol^{-1}, where the HCl E_{vib} distributions almost vanish. In the case of CH_2CN, there is a considerable fraction of vibrationally excited products, which is not surprising, since this polyatomic radical can be excited in several vibrational modes, including low-frequency torsional and bending modes. It is also interesting to note that the rotational and vibrational energies are comparable in magnitude for both products, indicating that the products are formed having significant rotation.

IV. SUMMARY AND CONCLUSIONS

In the present study, based on our previous work,[34] a full-dimensional analytical potential energy surface is automatically constructed for the Cl + CH_3CN system with the ROBOSURFER program,[35] developed in our group. A fifth-order permutationally invariant polynomial method is used for fitting the energy points calculated with a basis-set-corrected (cc-pVTZ-F12 – cc-pVDZ-F12) ManyHF-UCCSD(T)-F12a/cc-pVDZ-F12 level of theory and complemented also with SO correction. On the final PES quasi-classical trajectory simulations are performed to investigate the dynamics of the abstraction- and substitution pathways of the title reaction. However, the determined integral cross sections and reaction probabilities reveal that the substitution reaction probabilities are negligible in the applied collision energy range (10–60 kcal mol^{-1}); thus, further dynamics analyses are performed only for the hydrogen-abstraction channel. The QCT simulations also revealed an isomerization reaction pathway, resulting in CH_3NC + Cl products with an extremely low probability. The ICSs for H-abstraction increase with increasing collision energy, and the results show that ZPE violation is significant, especially if a hard constraint is used. The opacity functions show that the b parameter has a different impact on the reaction probability at different E_{coll}, which suggests that the direct stripping mechanism becomes more dominant with increasing collision energy. The maximum value of the impact parameter does not have an E_{coll} dependence. The indirect to direct stripping mechanism change is also supported by the scattering and attacking angle distributions. The former results in isotropic scattering at lower collision energies, and forward scattering gets more dominant with increasing E_{coll}. The distribution of initial attack angles shows a clear preference for the methyl group attack. At lower collision energies, the dominant attack angle is $\alpha = 70°$, pointing Cl toward one of the H atoms with a nearly collinear Cl–H–C arrangement, whereas at higher collision energies, the approach is mostly parallel to the C–C bond. Post-reaction energy distributions indicate that there is a greater transfer from the reactants' collision energy to the products' translational energy than to their internal energy. The dependence of the translational energy of the products on E_{coll} also supports our claim about the change in the directness of the reaction. According to the vibrational and rotational energy distributions, the HCl molecule is formed mostly in the ground vibrational state, but rotational excitement is significant, and neither of them shows a large collision energy dependence. In contrast, for the CH_2CN product, E_{coll} has a larger impact on E_{int}, which comes from the rotational energy. Both products are formed with significant rotating motion. The newly-developed PES creates the opportunity for further dynamics investigations that can be the subject of our future studies.

SUPPLEMENTARY MATERIAL

The supplementary material encompasses cross sections based on a different number of trajectories, numerical data for the opacity functions, fitting error distribution, comparison of the relevant PES and *ab initio* structural parameters of the stationary points, and codes (Ref. 41) and coefficients for PES evaluation.

ACKNOWLEDGMENTS

The authors thank the National Research, Development, and Innovation Office—NKFIH, K-146759; Project No. TKP2021-NVA-19, provided by the Ministry of Culture and Innovation of Hungary from the National Research, Development and Innovation Fund, financed under the TKP2021-NVA funding scheme; and the Momentum (Lendület) Program of the Hungarian Academy of Sciences for financial support. P. T. was supported by the ÚNKP-23-2 New National Excellence Program of the Ministry for Culture and Innovation from the source of the National Research, Development and Innovation Fund.

AUTHOR DECLARATIONS

Conflict of Interest

The authors have no conflicts to disclose.

Author Contributions

Petra Tóth: Data curation (lead); Formal analysis (lead); Investigation (lead); Methodology (lead); Visualization (lead); Writing – original draft (lead); Writing – review & editing (supporting). **Tímea Szűcs**: Data curation (supporting); Formal analysis (supporting); Investigation (supporting); Methodology (supporting); Software (supporting); Supervision (supporting); Validation (lead); Writing – review & editing (supporting). **Tibor Győri**: Investigation (supporting); Methodology (supporting); Software (lead); Writing – review & editing (supporting). **Gábor Czakó**: Conceptualization (lead); Funding acquisition (lead); Investigation (supporting); Methodology (supporting); Project administration (lead); Software (supporting); Supervision (lead); Validation (supporting); Writing – original draft (supporting); Writing – review & editing (lead).

DATA AVAILABILITY

The data that support the findings of this study are available from the corresponding author upon reasonable request.

REFERENCES

[1] C. Murray and A. J. Orr-Ewing, Int. Rev. Phys. Chem. **23**, 435 (2004).
[2] B. Jiang and H. Guo, J. Am. Chem. Soc. **135**, 15251 (2013).
[3] J. F. Castillo, F. J. Aoiz, and L. Bañares, J. Chem. Phys. **125**, 124316 (2006).
[4] S. J. Greaves, R. A. Rose, F. Abou-Chahine, D. R. Glowacki, D. Troya, and A. J. Orr-Ewing, Phys. Chem. Chem. Phys. **13**, 11438 (2011).
[5] S. T. Banks and D. C. Clary, Phys. Chem. Chem. Phys. **9**, 933 (2007).
[6] S. Yan, Y. T. Wu, B. Zhang, X.-F. Yue, and K. Liu, Science **316**, 1723 (2007).
[7] G. Czakó and J. M. Bowman, Science **334**, 343 (2011).
[8] F. Meng, W. Yan, and D. Y. Wang, Phys. Chem. Chem. Phys. **14**, 13656 (2012).
[9] B. Fu, X. Shan, D. H. Zhang, and D. C. Clary, Chem. Soc. Rev. **46**, 7625 (2017).
[10] Y. Liu and J. Li, Phys. Chem. Chem. Phys. **22**, 344 (2020).
[11] C. Rangel and J. Espinosa-Garcia, Phys. Chem. Chem. Phys. **20**, 3925 (2018).
[12] J. Espinosa-Garcia, E. Martinez-Nuñez, and C. Rangel, J. Phys. Chem. A **122**, 2626 (2018).
[13] D. Papp, V. Tajti, T. Győri, and G. Czakó, J. Phys. Chem. Lett. **11**, 4762 (2020).
[14] D. Papp and G. Czakó, J. Phys. Chem. A **126**, 2551 (2022).
[15] H. A. Bechtel, J. P. Camden, and R. N. Zare, J. Chem. Phys. **120**, 4231 (2004).
[16] D. Lu, J. Li, and H. Guo, CCS Chem. **2**, 882 (2020).
[17] C. Rangel and J. Espinosa-Garcia, Phys. Chem. Chem. Phys. **25**, 10678 (2023).
[18] S. Rudić, C. Murray, J. N. Harvey, and A. J. Orr-Ewing, Phys. Chem. Chem. Phys. **5**, 1205 (2003).
[19] T. Szűcs and G. Czakó, J. Chem. Phys. **159**, 134306 (2023).
[20] X. Xu and J. Li, J. Phys. Chem. A **126**, 6456 (2022).
[21] G. Poulet, G. Laverdet, J. L. Jourdain, and G. Le Bras, J. Phys. Chem. **88**, 6259 (1984).
[22] J. Olbregts, G. Brasseur, and E. Arijs, J. Photochem. **24**, 315 (1984).
[23] M. J. Kurylo and G. L. Knable, J. Phys. Chem. **88**, 3305 (1984).
[24] G. S. Tyndall, J. J. Orlando, T. J. Wallington, J. Sehested, and O. J. Nielsen, J. Phys. Chem. **100**, 660 (1996).
[25] G. S. Tyndall, J. J. Orlando, T. J. Wallington, and M. D. Hurley, J. Phys. Chem. A **105**, 5380 (2001).
[26] Q. S. Li and C. Y. Wang, J. Phys. Chem. A **106**, 8883 (2002).
[27] K. Pei and H. Li, J. Mol. Struct.: THEOCHEM **677**, 67 (2004).
[28] G. Markovich, L. Perera, M. L. Berkowitz, and O. Cheshnovsky, J. Chem. Phys. **105**, 2675 (1996).
[29] M. F. Rode, S. Roszak, J. J. Szymczak, J. Sadlej, and J. Leszczynski, J. Chem. Phys. **121**, 6277 (2004).
[30] D. J. Bogan and D. W. Setser, J. Chem. Phys. **64**, 586 (1976).
[31] D. Smith, D. W. Setser, K. C. Kim, and D. J. Bogan, J. Phys. Chem. **81**, 898 (1977).
[32] K. Dehe and H. Heydtmann, Chem. Phys. Lett. **262**, 683 (1996).
[33] S. Pratihar, X. Ma, J. Xie, R. Scott, E. Gao, B. Ruscic, A. J. A. Aquino, D. W. Setser, and W. L. Hase, J. Chem. Phys. **147**, 144301 (2017).
[34] P. Tóth, T. Szűcs, and G. Czakó, J. Phys. Chem. A **126**, 2802 (2022).
[35] T. Győri and G. Czakó, J. Chem. Theory Comput. **16**, 51 (2020).
[36] T. Győri and G. Czakó, J. Chem. Phys. **156**, 071101 (2022).
[37] G. Knizia, T. B. Adler, and H.-J. Werner, J. Chem. Phys. **130**, 054104 (2009).
[38] T. H. Dunning, Jr., J. Chem. Phys. **90**, 1007 (1989).
[39] K. A. Peterson, T. B. Adler, and H.-J. Werner, J. Chem. Phys. **128**, 084102 (2008).
[40] G. Knizia and H.-J. Werner, J. Chem. Phys. **128**, 154103 (2008).
[41] B. J. Braams and J. M. Bowman, Int. Rev. Phys. Chem. **28**, 577 (2009).
[42] S. R. Langhoff and E. R. Davidson, Int. J. Quantum Chem. **8**, 61 (1974).
[43] K. R. Shamasundar, G. Knizia, and H.-J. Werner, J. Chem. Phys. **135**, 054101 (2011).
[44] K. A. Peterson and T. H. Dunning, Jr., J. Chem. Phys. **117**, 10548 (2002).
[45] A. Berning, M. Schweizer, H.-J. Werner, P. J. Knowles, and P. Palmieri, Mol. Phys. **98**, 1823 (2000).
[46] H.-J. Werner, P. J. Knowles, G. Knizia, F. R. Manby, M. Schütz *et al.*, *Molpro, version 2015.1, a package of ab initio programs see* http://www.molpro.net.
[47] W. L. Hase, *Encyclopedia of Computational Chemistry* (Wiley, New York, 1998), pp. 399–407.